Appl Phys A (2013) 111:243–249
DOI 10.1007/s00339-013-7572-z

Applied Physics A
Materials Science & Processing

RAPID COMMUNICATION

Stable superhydrophobic surface with hierarchical mesh-porous structure fabricated by a femtosecond laser

Jiale Yong · Qing Yang · Feng Chen · Dongshi Zhang · Hao Bian · Yan Ou · Jinhai Si · Guangqing Du · Xun Hou

Received: 28 September 2012 / Accepted: 16 January 2013 / Published online: 29 January 2013

Abstract Inspired by the lotus leaf, a new superhydrophobic surface with hierarchical mesh-porous structure is fabricated by femtosecond laser irradiation on silicon. The fabricated surface shows a superhydrophobic character with water contact angle being found to reach up to $158° \pm 1°$ and sliding angle of $4° \pm 0.5°$. The superhydrophobicity is stable even if the PH of solution changes from 1 to 14. And the surface also exhibits excellent self-cleaning effect and bouncing behavior, implying that the adhesion of the surface is extremely low. This work will enhance further understanding of the wettability of a solid surface with special surface morphology.

1 Introduction

The wettability of a solid surface is an important property of materials which is governed by both the chemical composition and the physical morphology [1–3]. A superhydrophobic surface is characterized by the water contact angle (CA) larger than 150° and the sliding angle (SA) lower than 10°. The superhydrophobic surface has attracted much interest in fundamental research and practical applications, such as microfluidics, lab-on-chip devices, antisticking and low friction coatings [4–7]. In 1997, Barthlott and Neinhuis first revealed the underlying mechanism of water repellent property of the lotus leaf [8]. The lotus leaf surface is found to be completely covered by many micro-scale papillaes decorating with abundant nano-scale protrusions. Meanwhile, the epidermal cells on the lotus leaf surface are covered with an additional layer of epicuticular hydrophobic wax crystals with low surface free energy [9]. The combined action of the hierarchical rough structure and the chemical layer can minimize the real contact area between the surface and the droplet, leading to great enhancement of the superhydrophobicity of the lotus leaf [10, 11]. After scholars realized the unique structure of the lotus leaf, many efforts have been made in developing an artificial superhydrophobic surface by imitating the lotus leaf.

A surface with a super-water-repellent property can usually be achieved by creating a rough surface structure on a hydrophobic material or depositing a layer of chemical molecules with low surface free energy on a rough surface [12–18]. Though the repellent property of a surface can be enhanced by lowering the surface energy, as for a smooth surface, the greatest value is only about 120°. So structuring micro/nano-scale rough morphology along with chemical coating is the most suitable way to prepare artificial superhydrophobic surfaces [19]. So far, many techniques have been reported to produce superhydrophobic surfaces, including self-assembly, electrospinning, polymer imprinting, plasma-treated surfaces, lithography, and so on [20–26].

In recent years, micromachining by femtosecond laser has attracted much interest because it can not only produce the topography with two scale roughness via a one-step process, but can also be applied to a wide variety of materials, especially for high hardness, high brittleness, and other hard-cutting materials [27–31]. Furthermore, femtosecond laser micromachining enables the fabrication of true three-dimensional (3D) microstructures precisely, thus showing unique advantages over the traditional laser micromaching technology [32–36]. Controlled by a computer, complex

J. Yong · Q. Yang · F. Chen (✉) · D. Zhang · H. Bian · Y. Ou · J. Si · G. Du · X. Hou
State Key Laboratory for Manufacturing Systems Engineering & Key Laboratory of Photonics Technology for Information, School of Electronics & Information Engineering, Xi'an Jiaotong University, 710049, Xi'an, Shaanxi, China
e-mail: chenfeng@mail.xjtu.edu.cn

structures can be realized, exhibiting unique wetting property. T. Baldacchini et al. [37] and M. Barberoglou et al. [9], respectively, obtained excellent superhydrophobic Si surface by femtosecond laser irradiation under reactive gas (SF_6) atmosphere. But SF_6 gas makes the experiment equipment and process more complex, so it is important to explore how to prepare superhydrophobic surface in ambient environment using a femtosecond laser.

In this paper, we present an effective method to prepare superhydrophobic surface by a femtosecond laser on silicon in ambient environment. The silicon wafer is irradiated by femtosecond laser pulses and then coated by fluoroalkylsilane to lower the surface energy. The as-prepared surface shows a hierarchical mesh-porous structure, which is completely different from the surface irradiated under reactive gas (SF_6) atmosphere. The femtosecond laser irradiation results in a stable superhydrophobic surface with CA up to $158° \pm 1°$ and SA lower than $4° \pm 0.5°$. It is found that the as-prepared surface holds superhydrophobicity even though the CA has a slight rise and fall when the PH of solution changes from 1 to 14. In addition, the as-prepared surface also exhibits excellent self-cleaning effect and bouncing behavior.

2 Experimental

The material was a single crystal n-type Si (100) wafer with thickness of 0.5 mm and a resistivity of 6 Ω cm. The rough hierarchical micro/nano-scale binary structure was fabricated by femtosecond laser irradiation in ambient conditions on flat Si surface through a simple one-step process, and this method can be applied to a wide variety of materials. The schematic of the experimental setup is shown in [20]. A regenerative amplified Ti:sapphire laser system (Femtopower compact Pro) with a center wavelength of 800 nm was utilized and it could produce 30 fs pulses at a repetition rate of 1 kHz. A mechanical shutter was used as a switch to turn on and off the laser beam. The Gaussian laser beam (constant average power of 15 mW) was focused by a microscope objective lens (20×, NA = 0.45, Nikon) on the front side of the sample to a spot diameter of 10 μm. The sample was mounted on a motorized x–y–z translation stage controlled by a computer and positioned perpendicularly to the direction of laser incidence. In the experiment, a line-by-line and serial scanning process was used. The sample was irradiated at a scanning speed of 2 mm/s, and the interval of adjacent laser scanning lines was held constant at 2 μm. Since the laser repetition rate was 1 kHz, the adjacent distance of laser pulse focuses was 2 μm. Following the irradiation process, the sample was successively cleaned by acetone, alcohol, and deionized water in ultrasonic bath at room temperature for 10 minutes each time. Immediately afterwards, the sample was immersed into a 2 % fluoroalkylsilane solution for two hours in order to deposit a low surface free energy layer, and then it was roasted in a vacuum oven at 150 °C for another 4 hours to make the layer more stable.

The microstructure of the as-prepared surface obtained by a femtosecond laser was observed by an SEM-7000F scanning electron microscope (JOEL, Japan). The sizes of the holes and spikes and the surface roughness were measured by a LEXT OLS4000 laser confocal microscope (Olympus, Japan). The contact angle and the sliding angle of a 9 μl water droplet on the surface were measured by an OCA20 contact-angle system (Dataphysics, Germany) at ambient temperature, using a sessile drop method. The self-cleaning experiment was performed by placing a water droplet to roll across a slightly tilted structured surface which was equably strewed with calcium carbonate powder. PH change was achieved by gradually diluting concentrated sulfuric acid and sodium hydroxide solution. Finally, the bouncing behavior of a droplet free-falling on the as-prepared surface was investigated by the contact-angle system and a charge-coupled device (CCD) camera system to take photographs at 167 frames per second.

3 Results and discussion

Figures 1(a)–(d) show the typical scanning electron microscope (SEM) images of the as-prepared surface. The structured region is characterized by highly uniform hierarchical and periodic mesh-porous structure with the period of 10 μm. The average diameter and depth of the holes are about 8 and 4.6 μm, respectively. Each conical spike is surrounded by four holes, and the average diameter and height of the periodic conical spikes are about 6 and 2.9 μm, respectively. The surface roughness (R_a) is about 2.46 μm. The distance from the top of the spikes to the bottom of the holes can reach up to 7.5 μm. This large value makes the fabricated surface rough enough and is helpful to achieve superhydrophobicity.

Figures 1(e) and 1(f) show the images of a 9 μl water droplet lying on the surface irradiated by a femtosecond laser. The static contact angle on the as-prepared surface is as high as $158° \pm 1°$ while the sliding angle is lower than $4° \pm 0.5°$, indicating that the water droplet can move very easily even when the surface is only slightly tilted or shaken. Figure 2 shows a time sequence of snapshots of a water droplet rolling on a 4° tilted structured surface. Both the high CA and the low SA demonstrate that the as-prepared surface has outstanding character of superhydrophobicity and the dual-scale hierarchical structure is very important to enhance the hydrophobicity of the surface.

The micro- and nanostructures of the fabricated surface are caused by the ablation under laser pulses and the recrystallization of ejected particles, respectively. When the

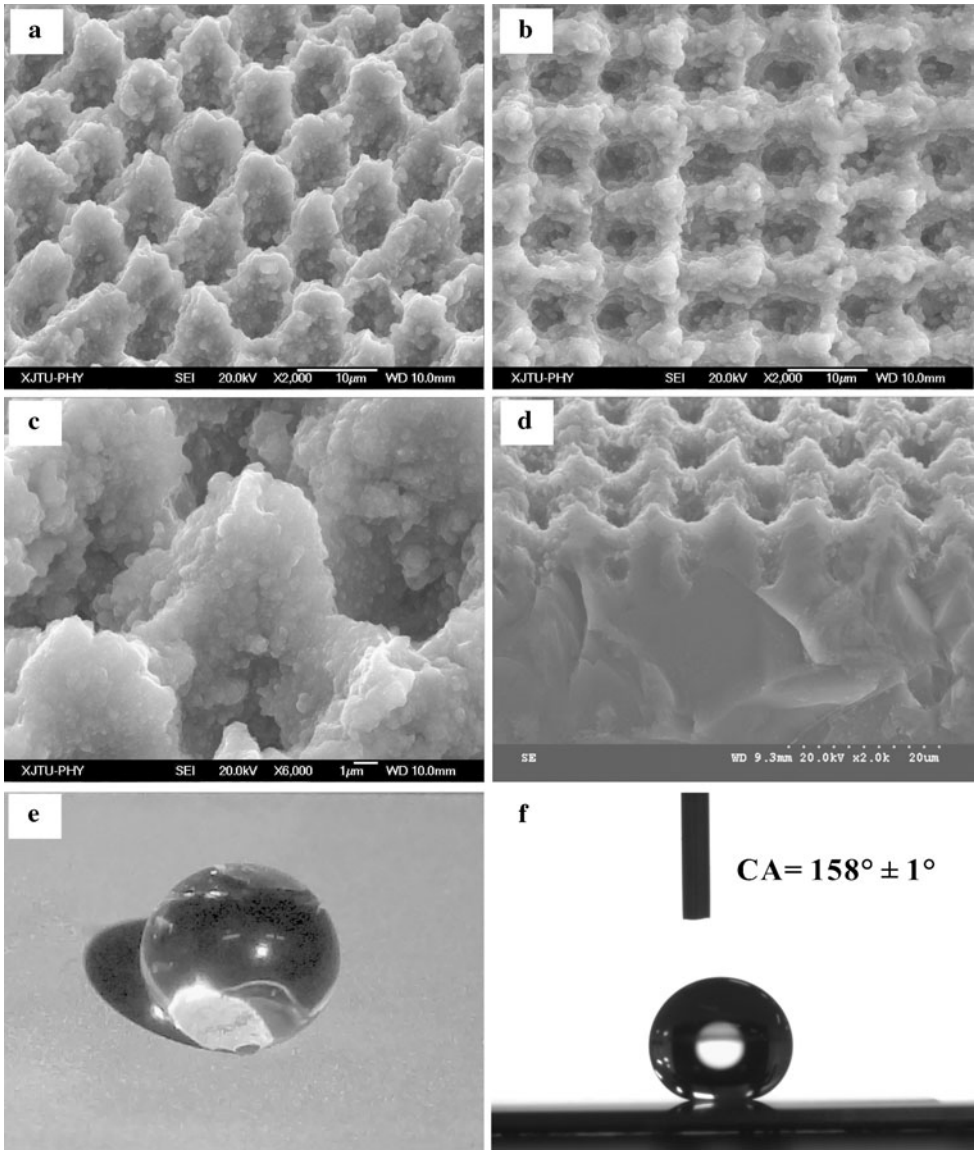

Fig. 1 Typical SEM images of the structure irradiated by femtosecond laser: (**a**) side-view SEM, (**b**) top-view SEM, (**c**) higher resolution SEM, and (**d**) cross-sectional SEM. (**e**)–(**f**) Shapes of a 9 μl water droplet on the as-prepared surface with a contact angle of 158° ± 1°

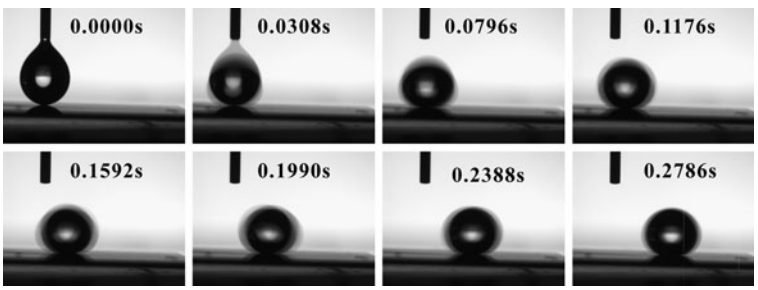

Fig. 2 Time sequence of snapshots of a water droplet rolling on the 4° tilted surface

fluence of incoming femtosecond laser pulses is higher than the damage threshold of silicon, part of the incident laser energy is absorbed initially by electrons through the nonlinear effects such as multiphoton and avalanche ionization [38]. Meanwhile, the electrons transfer some energy to the lattice. As the electrons and ions thermally equilibrate, high-pressure and high-temperature plasma is formed above the surface. The plasmas expand and burst out of the focal spot, and the ablated materials are removed from the surface [39, 40]. Figure 3 shows a series of SEM images of the structured silicon surface irradiated by femtosecond laser at scanning rows (N) of 1–5, 7, 10, and 20. After the first row of femtosecond laser scanning, periodic holes decorating with ridges between them appear on the silicon surface, as shown

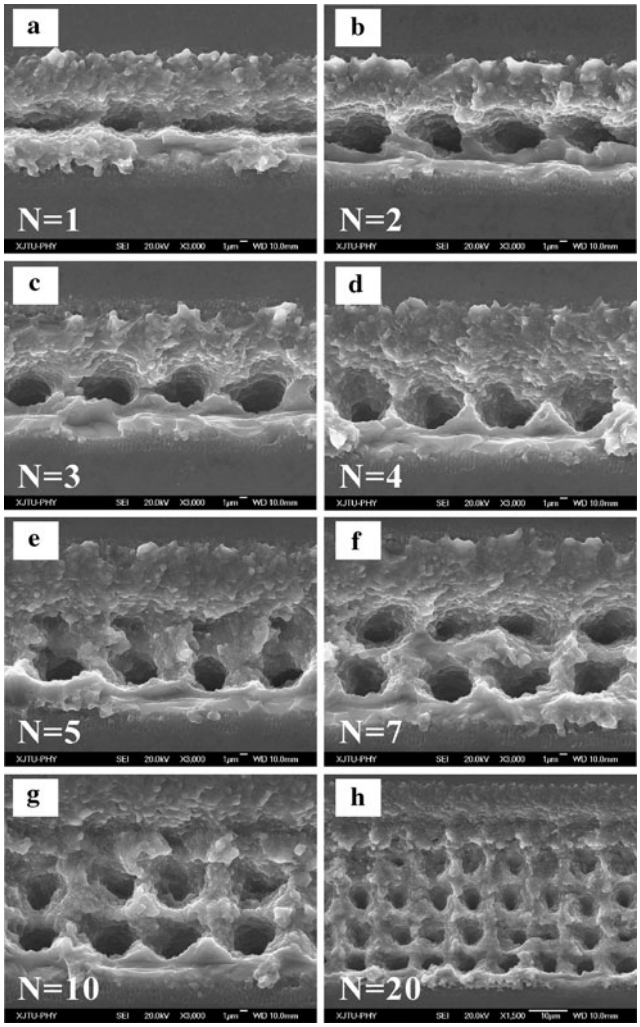

Fig. 3 Scanning electron micrographs of a silicon surface irradiated by femtosecond laser at different scanning rows (N). The canning speed is 2000 μm/s and the interval of adjacent rows is 2 μm. The scanning rows are added upward in the longitudinal direction

in Fig. 3(a). The period is about 10 μm. Since the distance of the adjacent pulse focuses is 2 μm, a hole is produced as the result of overlapping of five femtosecond laser pulses. When the silicon is irradiated by a pulse, ejected particles will be stacked out of the crater and form a recast layer. The recast layer will be pushed forward and accumulate on the moving direction. When the fifth pulse is outputted, the recast layer is hard to move forward because it is thick enough due to the cumulative effect. At this time, the pulse cannot cause more serious damage to the silicon surface because of the interference from the recast layer. As the laser focus continues to move forward and passes over the recast layer, the sixth laser pulse is back to the original processing plane. And the sixth to tenth pulses will lead to a new hole and a new recast layer similar to the formation of the first hole. This process repeats and the periodic hole structure can be formed by a single row of scanning. On the other hand, longitudinal forming process is similar to the transverse forming process, as shown in Figs. 3(b)–(e). When N equals 5, the first row of periodic holes is completely induced and the sign of the second row is emerging (Fig. 3(e)). In addition, tens or hundreds of nanometer-sized protrusions self-assemble at the edge of the holes for the re-crystallization of ejected particles [30]. Further increase in N will give rise to the second row of the periodic holes (Figs. 3(f) and 3(g)). Following the same process shown in Figs. 3(a)–(e), the hierarchical mesh-porous structure is fabricated by femtosecond laser irradiation on silicon when the scanning rows are large enough (Fig. 3(h)).

The contact angle on the hierarchical surface can be expressed by the Cassie–Baxter equation [41, 42]:

$$\cos\theta_c = f\cos\theta + f - 1 \tag{1}$$

where θ_c and θ are the contact angles of the as-prepared surface and the flat silicon coating fluoroalkylsilane solution, respectively. f is the fraction of the surface which is in contact with the liquid. According to (1), the value of f of the as-prepared surface can be inferred to be 0.111 ($\theta_c = 158°$ and $\theta = 110°$), which indicates that the droplet only contacts a small area of the rough surface. The air, which is filled in the interspaces between the droplet and the as-prepared surface, is an ideal superhydrophobic material and results in the superhydrophobicity of the as-prepared surface.

Figure 4 shows the shapes of a droplet on the different types of morphology. For simplicity, we assume that the liquid touches just the top of the surface. In Figs. 4(a) and 4(b), the surfaces only have microscale and nanoscale structures, respectively. Combining the two above structures, a new surface with micro- and nanoscale hierarchical structure is obtained, as show in Fig. 4(c). Thus the Cassie–Baxter equation of a droplet on these three kinds of surfaces can be expressed as (assuming that the materials of the three substrates are the same and the intrinsic contact angles are all θ):

$$\cos\theta_1 = f_1(\cos\theta + 1) - 1, \tag{2}$$

$$\cos\theta_2 = f_2(\cos\theta + 1) - 1, \tag{3}$$

$$\cos\theta_3 = f_3(\cos\theta + 1) - 1, \tag{4}$$

where θ_1, θ_2, and θ_3 are the measured contact angles and f_1, f_2, and f_3 are area fractions of the solid–liquid interface when a water droplet on the surface with just microscale structure, just nanoscale structure, and micro- and nanoscale hierarchical structure, respectively. It is easy to see that $f_3 = f_1 \times f_2$. And then (4) can be changed as follows:

$$\cos\theta_3 = f_1 f_2(\cos\theta + 1) - 1. \tag{5}$$

According to the definition, $0 < f_1, f_2, f_3 < 1$. When $\theta > 90°$, implying that the material of the three substrates is hydrophobic for water, it is easy to find that $\cos\theta_1$, $\cos\theta_2$, and

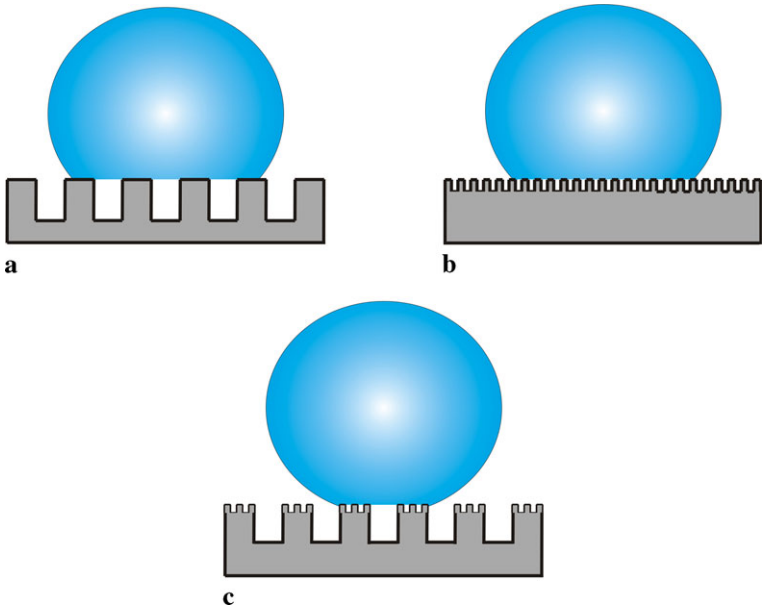

Fig. 4 Shapes of a water droplet on the surface with (**a**) just microscale structure, (**b**) just nanoscale structure, and (**c**) micro- and nanoscale hierarchical structure

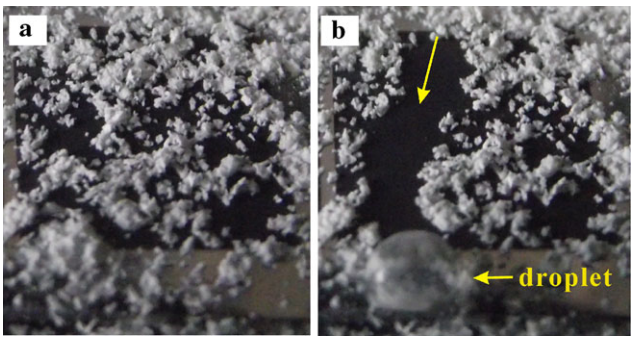

Fig. 5 Images of a 10 μl water droplet rolling across the as-prepared surface which was tilted by a small angle and equably strewed with calcium carbonate powder treated as a pollutant

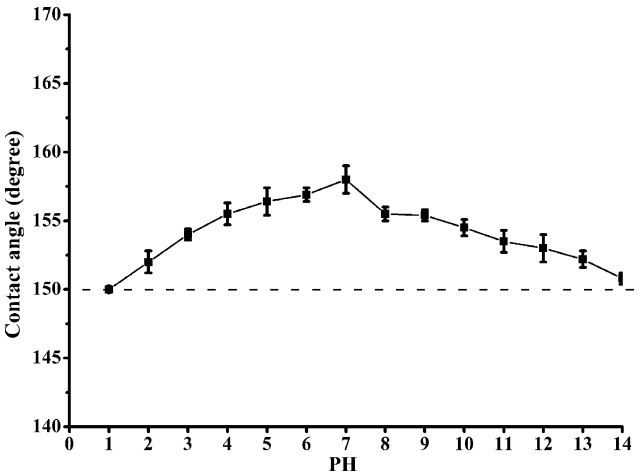

Fig. 6 Relationship between contact angle and PH of liquid on the as-prepared surface

$\cos\theta_3$ are all less than 0. By (2) and (5), we simply get the inequality:

$$\cos\theta_3 = f_1 f_2(\cos\theta + 1) - 1 < f_1(\cos\theta + 1) - 1$$
$$= \cos\theta_1 < 0$$
$$\text{(due to } 0 < f_2 < 1\text{)}$$

so that $\theta_3 > \theta_1 > 90°$. Also we can obtain $\theta_3 > \theta_2 > 90°$. In other words, we can get $\theta_3 > \theta_1, \theta_2 > \theta > 90°$ for an intrinsically hydrophobic material. This relationship declares that single micro- and nanoscale roughness can enhance the hydrophobicity, and the micro- and nanoscale hierarchical structure leads to greater improvement in water repellent property than the single micro- or nanoscale rough surface. Obviously, a multi-level rough structure is more effective than a single micro- or nanoscale rough surface to decrease the area fraction of the solid–liquid interface or increase the area fraction of the solid–air interface, and this is the main reason for a better achieved superhydrophobicity.

In order to investigate the self-cleaning ability of the as-prepared surface, calcium carbonate powder is strewed on the slightly tilted surface, acting as a pollutant. A 10 μl water droplet is located on the surface to roll off. It can be clearly seen that the primal surface covering with pollutant is very messy (Fig. 5(a)), but the path where the water droplet crossed is clean with nearly no pollutant left (Fig. 5(b)). Meanwhile, the droplet becomes muddy since it collects all of calcium carbonate powder on the path. This indicates that the surface fabricated by femtosecond laser exhibits fine self-cleaning ability [11].

Interestingly, the CAs of the as-prepared surface are larger than 150° for not only water but also for corrosive

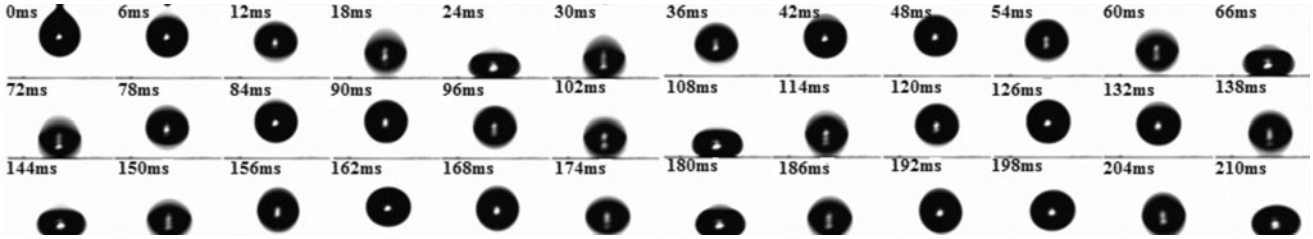

Fig. 7 Time sequence of snapshots of a 10 µl water droplet free-falling and impacting the as-prepared surface

liquids, such as acid and alkaline and other basic aqueous solutions. This property makes the superhydrophobic surface suitable to be applied more widely and more flexibly. The as-prepared surface still has a self-cleaning function even in acid or alkaline rain. Figure 6 shows the relationship between CA and PH on the superhydrophobic surface. When the PH is tuned from 1 to 7, the CAs increase from about $150° \pm 0.2°$ to $158° \pm 1°$, while the CAs decrease from $158° \pm 1°$ to $150.8° \pm 0.4°$ when the PH increases from 7 to 14. Clearly, this fluctuation is negligible and all the CAs are equal or higher than 150°, indicating that the as-prepared surface shows stable superhydrophobic property in a wide PH range from 1 to 14, which is not easily attained by many other artificial superhydrophobic surfaces. This PH stable superhydrophobicity is very important for the use of the surface irradiated by femtosecond laser in chemical and biological fields.

Figure 7 presents a time sequence of snapshots with a 10 µl water droplet free-falling and impacting on the as-prepared surface. The droplet is released by a glass microsyringe at ambient condition from a height of 3 mm. As is shown in the images, after contacting the as-prepared surface, the droplet deformed into a flat ellipsoid at first, then recovered quickly, and finally rebounded off the surface. Meanwhile, it is shown that the shape of the water droplet changes observably during impact because its kinetic energy transforms into internal energy and vibration energy due to surface deformation. The droplet can bounce numerous times and remain completely intact despite ruthlessly impacting the surface of the sample. The impact of air resistance can be ignored because the volume and height of the free-falling water droplet are small. This way, the v' and v (the center of mass velocity just after impact and just before impact) can be approximately expressed as $\sqrt{2h'/g}$ and $\sqrt{2h/g}$, respectively. h' is the height of rebound, and h is the height of falling. They can be deduced from the recorded snapshots. So the simplified rebound coefficient (the ratio of the center of mass velocity just after impact to that just before impact) can be expressed as $k = \frac{v'}{v} = \sqrt{\frac{h'}{h}}$. According to Fig. 7, the coefficient stabilizes near 0.9 for each bounce, and such a high value reveals an excellent superhydrophobicity of the as-prepared surface [43, 44].

4 Conclusions

In conclusion, the superhydrophobic surface was fabricated by a femtosecond laser on silicon. The as-prepared surface shows hierarchical mesh-porous structure with both micro/nano-scale roughnesses. The contact angle can reach up to $158° \pm 1°$ and the sliding angle is lower than $4° \pm 0.5°$. Importantly, the surface shows stable superhydrophobicity over a wide pH range. This property enables the superhydrophobic surface to have a self-cleaning function even in acid or alkaline rain. In addition, the as-prepared surface also exhibits excellent bouncing behavior with a rebound coefficient of 0.9 for each bounce. The presented technique is simple and can accurately control the processing location, which is an important supplement to the traditional chemical and simple mechanical methods.

Acknowledgements This work is supported by National Science Foundation of China under the Grant Nos. 61176113, 61275008 and the Fundamental Research Funds for the Central Universities.

References

1. X. Yao, Y.L. Song, L. Jiang, Adv. Mater. **23**, 719–734 (2011)
2. T. Verho, C. Bower, P. Andrew, S. Franssila, O. Ikkala, R.H.A. Ras, Adv. Mater. **23**, 673–678 (2011)
3. X.M. Li, D. Reinhoudt, M.C. Calama, Chem. Soc. Rev. **36**, 1350–1368 (2007)
4. W. Song, D.D. Veiga, C.A. Custodio, J.F. Mano, Adv. Mater. **21**, 1830–1834 (2009)
5. Z. Wang, C. Lopez, A. Hirsa, N. Koratkar, Appl. Phys. Lett. **91**, 023105 (2007)
6. S. Gou, M. Mossman, L. Whitehead, Appl. Opt. **51**(11), 1645–1653 (2012)
7. F. Xia, L. Jiang, Adv. Mater. **20**, 2842–2858 (2008)
8. W. Barthlott, C. Neinhuis, Planta **202**, 1–8 (1997)
9. M. Barberoglou, V. Zorba, E. Stratakis, P. Tzanetakis, S.H. Anastasiadis, C. Fotakis, Appl. Surf. Sci. **255**, 5425–5429 (2009)
10. V. Zorba, E. Stratakis, M. Barberoglou, E. Spanakis, P. Tzanetakis, S.H. Anastasiadis, C. Fotakis, Adv. Mater. **20**, 4049–4054 (2008)
11. J. Genzer, K. Efimenko, Biofouling **22**, 339–360 (2006)
12. Z.G. Cheng, L. Feng, L. Jiang, Adv. Funct. Mater. **18**, 3219–3225 (2008)
13. L. Feng, S. Li, Y. Li, Adv. Mater. **14**, 1857–1860 (2002)
14. Z.G. Guo, F. Zhou, J.C. Hao, W.M. Liu, J. Am. Chem. Soc. **127**, 15670–15671 (2005)
15. Y.K. Lai, X.F. Gao, H.F. Zhuang, J.Y. Huang, C.G. Lin, L. Jiang, Adv. Mater. **21**, 3799–3803 (2009)

16. I. Banerjee, R.C. Pangule, R.S. Kane, Adv. Mater. **23**, 690–718 (2011)
17. X. Zhang, F. Shi, J. Niu, Y.G. Jiang, Z.Q. Wang, J. Mater. Chem. **18**, 621–633 (2008)
18. L. Coriand, M. Mitterhuber, A. Duparré, A. Tünnermann, Appl. Opt. **50**(9), C257–C263 (2011)
19. N.J. Shirtcliffe, S. Aqil, C. Evans, G. Mchale, M.I. Newton, C.C. Perry, P. Roach, J. Micromech. Microeng. **14**, 1384–1389 (2004)
20. F. Chen, D.S. Zhang, Q. Yang, X.H. Wang, B.J. Dai, J.H. Si, X. Hou, Langmuir **21**, 359–365 (2011)
21. D.S. Zhang, F. Chen, Q. Yang, J.H. Si, X. Hou, Soft Matter **7**, 8337–8342 (2011)
22. J.H. Zhang, Y.Y. Li, X.M. Zhang, B. Yang, Adv. Mater. **22**, 4249–4269 (2010)
23. D.G. Shchukin, E. Skorb, V. Belova, H. Mohwald, Adv. Mater. **23**, 1922–1934 (2011)
24. D. Zahner, J. Abagat, F. Svec, J.M.J. Frechet, P.A. Levkin, Adv. Mater. **23**, 3030–3034 (2011)
25. B. Cortese, S. D'Amone, M. Manca, I. Viola, R. Cingolani, G. Gigli, Langmuir **24**, 2712–2718 (2008)
26. R.B. Pernites, R.R. Ponnapati, R.C. Advincula, Adv. Mater. **23**, 3207–3213 (2011)
27. X.H. Wang, F. Chen, H.W. Liu, W.W. Liang, Q. Yang, J.H. Si, X. Hou, Opt. Commun. **284**, 317–321 (2011)
28. J. Bonse, K.W. Brzeinka, A.J. Meixner, Appl. Surf. Sci. **221**, 215–230 (2004)
29. D.S. Zhang, F. Chen, J.Z. Shi, H.W. Liu, H. Wang, J.H. Si, X. Hou, Ferroelectrics **387**, 130–136 (2009)
30. J. Bonse, S. Bandach, J. Kruger, W. Kautek, M. Lenzer, Appl. Phys. A **74**, 19–25 (2002)
31. M. Zhou, H.F. Yang, B.J. Dai, J.K. Di, E.L. Zhao, L. Cai, Appl. Phys. A **94**, 571–576 (2009)
32. M.Y. Shen, C.H. Crouch, J.E. Carey, E. Mazur, Appl. Phys. Lett. **85**(23), 5694–5696 (2004)
33. R. Le Harzic, H. Schuck, D. Sauer, T. Anhut, I. Riemann, Opt. Express **13**, 6651–6656 (2005)
34. H.W. Liu, F. Chen, X.H. Wang, Q. Yang, H. Bian, J.H. Si, X. Hou, Thin Solid Films **518**, 5188–5194 (2010)
35. G. Daminelli, J. Kruger, W. Kautek, Thin Solid Films **467**, 334–341 (2004)
36. D.S. Zhang, F. Chen, H.W. Liu, X.H. Wang, K. Du, J.H. Si, X. Hou, Chin. Sci. Bull. **55**, 877–881 (2010)
37. T. Baldacchini, J.E. Carey, M. Zhou, E. Mazur, Langmuir **22**, 4917–4929 (2006)
38. D. von der Linde, K. Sokolowski-Tinten, J. Bialkowski, Appl. Surf. Sci. **109**, 1–10 (1997)
39. A. Ben-Yakar, A. Harkin, J. Ashmore, R. Byer, H.A. Stone, J. Phys. D, Appl. Phys. **40**, 1447–1459 (2007)
40. B. Hao, H.W. Liu, F. Chen, Q. Yang, P.B. Qu, G.Q. Du, J.H. Si, X.H. Wang, X. Hou, Opt. Express **20**, 12939–12948 (2012)
41. L. Feng, S.H. Li, H.J. Li, J. Zhai, Y.L. Song, L. Jiang, D.B. Zhu, Angew. Chem. **114**, 1269–1271 (2002)
42. A.B.D. Cassie, S. Baxter, Trans. Faraday Soc. **40**, 546–551 (1944)
43. D. Richard, D. Quere, Europhys. Lett. **50**(6), 769–775 (2000)
44. A.L. Boance, F. Chevy, C. Clanet, G. Lagubeau, D. Quere, J. Fluid Mech. **554**, 47–66 (2006)